Langmuir
Article
pubs.acs.org/Langmuir

Microtextured Surfaces with Gradient Wetting Properties

Kevin R. Langley and James S. Sharp*

School of Physics and Astronomy and Nottingham Nanotechnology and Nanoscience Centre, University of Nottingham, University Park, Nottingham NG7 2RD, U.K.

Received July 30, 2010. Revised Manuscript Received October 5, 2010

Patterned surfaces with microwrinkled surface structures were prepared by thermally evaporating thin aluminum (10−300 nm thick) (Al) layers onto thick prestrained layers of a silicone elastomer and subsequently releasing the strain. This resulted in the formation of sinusoidal periodic surface wrinkles with characteristic wavelengths in the 3−42 μm range and amplitudes as large as 3.6 ± 0.4 μm. The Al thickness dependence of the wrinkle wavelengths and amplitudes was determined for different values of the applied prestrain and compared to a recent large-amplitude deflection theory of wrinkle formation. The results were found to be in good agreement with theory. Samples with spatial gradients in wrinkle wavelength and amplitude were also produced by applying mechanical strain gradients to the silicone elastomer layers prior to deposition of the Al capping layers. Sessile water droplets that were placed on these surfaces were found to have contact angles that were dependent upon their position. Moreover, these samples were shown to direct the motion of small water droplets when the substrates were vibrated.

Introduction

Spontaneous pattern-formation processes in thin films provide a valuable method for the production of surfaces with well-defined spatial variations in topography. The processes that underlie the formation of these spectacular patterns are usually governed by an underlying physical instability whose evolution results in the selection of a characteristic wrinkling length scale. This length scale is often determined as the result of a compromise between two or more competing physical processes that favor structure formation on different length scales. In each case the details of the pattern-formation process vary, but the results are often very similar in terms of the morphology of the surface structures that are produced and the length scales that are associated with the characteristic wavelengths and amplitudes of the structures that form. The lateral sizes/wavelengths of the structures that form are typically in the submicrometer to hundreds of micrometers range, and the amplitudes vary from a few nanometers up to a few micrometers. The production of structured surfaces with features on these technologically relevant length scales has resulted in them finding applications in the manufacture of stretchable electronics,[1] microfluidic devices,[2] substrates for cell adhesion,[3] and surfaces for the separation of particles with different sizes.[4] They have also been used to measure the mechanical properties of thin films[5] and to manufacture optical components such as diffraction gratings and optical diffusers.[6,7]

Pattern-formation processes that involve the bending of a rigid capping layer have been a key area of research because of the availability of a wide range of techniques (such as thermal evaporation, sputtering, and spin coating) that enable researchers to deposit ultrathin films of a material with well-defined thickness and uniformity onto solid substrates. In these pattern-formation processes, the mismatch in physical properties between the capping layer and an underlying layer or substrate is used to create a differential response of the layers in response to an applied stimulus. In many ways, the physics that underlies these processes is very similar to that which describes the operation of a simple bimetallic strip. However, the confinement of the capping layer and underlying layers by a substrate often prevents the samples from bending macroscopically, and the samples try to relieve the stresses that are exerted on them (as a result of the differential response of the layers) by wrinkling with a characteristic wavelength that typically lies in the micrometers to hundreds of micrometers range. This length scale is often significantly shorter than the lateral dimensions of the samples and is determined by a subtle balance of the in-plane stresses that are generated when an external stimulus is applied and the bending stresses that arise in the rigid capping layers when they deform. The in-plane stresses that develop in the samples can be generated by applying changes in temperature to samples with layers that have different thermal expansion coefficients.[8] They can also be driven by the differential response of the layers to a swelling solvent[9] or an applied mechanical stress.[4,10−12] Other authors have used changes in the roughness of an interface between two materials to drive the instabilities that result in the formation of periodic surface patterns.[13,14] A significant amount of experimental work has also been focused on the formation of surface structures on silicone elastomers that are coated with a rigid capping layer. The capping layers are usually deposited using thermal evaporation techniques[4,8,10−12,15,16] or by chemical modification of the surface

*Corresponding author. E-mail: james.sharp@nottingham.ac.uk.

(1) Sun, Y.; Choi, W. M.; Jiang, H.; Rogers, J. A. *Nat. Nanotechnol.* **2006**, *1*, 201–207.
(2) Stroock, A. D.; Whitesides, G. M. *Acc. Chem. Res.* **2003**, *36*, 597–604.
(3) Lam, M. T.; Clem, W. C.; Takayama, S. *Biomaterials* **2008**, *29*, 1705–1712.
(4) Effimenko, K.; Rackaitis, M.; Manias, E.; Vaziri, A.; Mahadevan, L.; Genzer, J. *Nat. Mater.* **2005**, *4*, 293–297.
(5) Stafford, C. M.; et al. *Nat. Mater.* **2004**, *3*, 545–550.
(6) Bowden, N.; Huck, W. T. S.; Paul, K. E.; Whitesides, G. M. *Appl. Phys. Lett.* **1999**, *75*, 2557–2559.
(7) Wang, J.; et al. *Opt. Laser Technol.* **2009**, *41*, 804–808.
(8) Bowden, N.; Brittain, S.; Evans, A. G.; Hutchinson, J. W.; Whitesides, G. M. *Nature* **1998**, *393*, 146–149.
(9) Sharp, J. S.; Jones, R. A. L. *Adv. Mater.* **2002**, *14*, 799–802.
(10) Ohzono, T.; Shimomura, M. *Phys. Rev. B* **2004**, *69*, 132202.
(11) Ohzono, T.; Shimomura, M. *Phys. Rev. E* **2005**, *72*, 025203(R).
(12) Ohzono, T.; Shimomura, M. *Langmuir* **2005**, *21*, 7230–7237.
(13) Sharp, J. S.; Vader, D.; Forrest, J. A.; Smith, M. I.; Khomenko, M.; Dalnoki-Veress, K. *Eur. Phys. J. E* **2006**, *19*, 423–432.
(14) Sharp, J. S.; Thomas, K. R.; Weir, M. P. *Phys. Rev. E* **2007**, *75*, 011601.
(15) Chen, X.; Hutchinson, J. W. *J. Appl. Mech.* **2004**, *71*, 597–603.
(16) Genzer, J.; Groenewold, J. *Soft Matter* **2006**, *2*, 310–323.

of the elastomer,[6,7,17,18] and the patterns are formed by changes in the temperature of the samples or by the application of mechanical stress.

Numerous attempts have been made to derive theories that explain and predict the length scales that are associated with spontaneous pattern-formation processes. A number of theories have been developed to describe pattern formation in systems where the length scales are formed by a mismatch in thermal expansion coefficients,[8,19,20] applied mechanical strains,[21] roughness-induced instabilities,[13,14] and dispersion-driven morphologies.[22] However, many of these theories assume a linear stability approach, and as a result, they often consider only small-amplitude deflections at the surfaces of the samples. This can result in errors when these theories are applied to situations where the amplitude of surface deflections is comparable to (or larger than) the thickness of one or more of the layers in the system. This has prompted the development of a number of more detailed theories of thin film wrinkling such as those developed by Huang, Suo, and co-workers[23−26] and Song et al.[27]

Surfaces with gradient wetting properties have recently received a great deal of attention because of their ability to direct the motion of small liquid droplets. Control of the wetting properties on these surfaces is often achieved using gradients in chemical properties.[28] These chemically patterned gradient surfaces have been shown to exhibit both spontaneous droplet motion[28] and driven droplet motion.[29] An alternative approach to the production of gradient surfaces is to use topographically patterned substrates. In these experiments, chemically uniform surfaces were patterned with periodic surface structures on different length scales. This was shown to change the contact angles formed by sessile water droplets that were placed on the surfaces of these samples.[30] Recent studies have shown that the contact angles that are formed by water droplets on surface-patterned elastomers are influenced by the amplitudes and wavelengths of 1D surface grooves.[30] Moreover, these studies revealed that the contact angles that are observed on these surfaces differ depending on whether the droplets are viewed parallel or perpendicular to the groove axes. These interesting wetting phenomena occur because of changes in the balance of interfacial energies that are experienced by a sessile droplet. For example, a droplet on a topographically patterned surface experiences a much larger contact area than a droplet with the same basal radius on a flat surface. This means that the energy associated with the contact region between the drop and the surface is larger than it would be on a corresponding flat surface. This increase in the liquid/substrate interfacial energy component is unfavorable, and the droplet can often reduce its total interfacial/surface energy by increasing the area of the liquid/air interface, thus altering its shape.[30] This can have a profound effect on the three-phase contact angle at the liquid/air/substrate interface. Under extreme circumstances, this can result in contact angles as large as 180° and the production of superhydrophobic or "self-cleaning" surfaces.[31] The sensitivity of surface wetting properties to local topography has also led researchers to develop lithographically patterned surfaces that have topography gradients where the characteristic length scale associated with the surface structures varies with position on the sample. This was shown to result in gradients in the wetting properties of the substrates that assist in driving the motion of small droplets across the patterned surfaces.[32]

In this article, we describe an experimental study of wrinkle formation in Al/silicone elastomer bilayers that are subjected to an applied mechanical prestrain. The Al thickness dependence of the wrinkling amplitude and wavelength is determined for different values of the applied prestrain, and the results are compared to a theory of wrinkle formation that was recently developed by Song et al.[27] These authors showed that in the limit of large deflections, the wavelength, λ, and amplitude, A, of the sinusoidal surface wrinkles that are produced when a prestrain, ε_{pre}, is applied to an elastomer with a thin solid coating of thickness h_{cap} are given by

$$\lambda = \frac{2\pi h_{cap}\left[\frac{E_{cap}(1-\nu_{sub}{}^2)}{3E_{sub}(1-\nu_{cap}{}^2)}\right]^{1/3}}{(1+\varepsilon_{pre})\left(1+\frac{5\varepsilon_{pre}(1+\varepsilon_{pre})}{32}\right)^{1/3}} \quad (1)$$

$$A = h_{cap}\frac{\sqrt{4\varepsilon_{pre}\left(\frac{E_{cap}(1-\nu_{sub}{}^2)}{3E_{sub}(1-\nu_{cap}{}^2)}\right)^{2/3}-1}}{\sqrt{1+\varepsilon_{pre}}\left(1+\frac{5\varepsilon_{pre}(1+\varepsilon_{pre})}{32}\right)^{1/3}} \quad (2)$$

where E_{cap}, E_{sub}, ν_{cap}, and ν_{sub} are the Young's modulii and Poisson ratios of the solid capping layer and elastomeric substrate, respectively. Song et al. confirmed the validity of their model by considering the effects of prestrain on poly(dimethylsiloxane) (PDMS)−silicon bilayer structures. To our knowledge, there are no further studies exploring the parameters that govern the sizes of the wrinkles produced by this method in other systems and with different capping-layer materials.

We show that this theory is in good agreement with our experimental results. We also present data on samples that have been manufactured in such a way that a strain gradient is applied to the elastomer prior to the deposition of the Al capping layers. When the mechanical strain is released, these bilayer samples are shown to have a gradient in wrinkle wavelength and amplitude across the samples. This gradient in length scales is shown to result in a gradient in wetting properties, with small water droplets displaying different contact angles at different positions on the samples. To the best of our knowledge, these are the first studies where good quantitative agreement is obtained between theory and experiments for mechanically driven pattern-formation processes in Al-capped elastomers. The use of thin film instabilities to create surfaces with gradients in topography and wettability is also the first of its kind. Although previous studies have considered

(17) Huck, W. T. S.; Bowden, N.; Onck, P.; Pardoen, T.; Hutchinson, J. W.; Whitesides, G. M. *Langmuir* **2000**, *16*, 3497–3501.
(18) Shih, T.; Ho, J.; Chen, C.; Whang, W.; Chen, C. *Appl. Surf. Sci.* **2007**, *253*, 9381–9386.
(19) Yoo, P. J.; Lee, H. H. *Phys. Rev. Lett.* **2003**, *91*, 154502.
(20) Yoo, P. J.; Suh, K. Y.; Kang, H.; Lee, H. H. *Phys. Rev. Lett.* **2004**, *93*, 034301.
(21) Sridhar, N.; Srolovitz, D. J.; Suo, Z. *Appl. Phys. Lett.* **2001**, *78*, 2482–2484.
(22) Dalnoki-Veress, K.; Nickel, B. G.; Dutcher, J. R. *Phys. Rev. Lett.* **1999**, *82*, 1486.
(23) Huang, R.; Suo, Z. *J. Appl. Phys.* **2002**, *91*, 1135–1142.
(24) Huang, R.; Suo, Z. *Int. J. Solids Struct.* **2002**, *39*, 1791–1802.
(25) Huang, R. *J. Mech. Phys. Solids* **2005**, *53*, 63–89.
(26) Im, S. H.; Huang, R. *J. Appl. Mech.* **2005**, *72*, 955–961.
(27) Song, J.; Jiang, H.; Liu, Z. J.; Khang, D. Y.; Huang, Y.; Rogers, J. A.; Lu, C.; Koh, C. G. *Int. J. Solids Struct.* **2008**, *45*, 3107–3121.
(28) Chaudhury, M. K.; Whitesides, G. M. *Science* **1992**, *256*, 1539–1541.
(29) Daniel, S.; Sircar, S.; Gliem, J.; Chaudhury, M. K. *Langmuir* **2004**, *20*, 4085–4092.
(30) Chung, J. Y.; Youngblood, J. P.; Stafford, C. M. *Soft Matter* **2007**, *3*, 1163–1169.
(31) Cheng, Y. T.; Rodak, D. E.; Wong, C. A.; Hayden, C. A. *Nanotechnology* **2006**, *17*, 1359–1362.
(32) Shastry, A.; Case, M. J.; Bohringer, K. F. *Langmuir* **2006**, *22*, 6161–6167.

pattern/wrinkle formation in similar systems, the patterns that form have a uniform length scale across the surface of the sample.[4,6,8,13,16,17] The present study describes a novel and facile method of producing samples with a gradient in wrinkle length scales that act as gradient energy surfaces for the biased transport of small liquid droplets.

Experimental Section

Thick films of a flowable silicone elastomer (RS Components Ltd., U.K.) were cast by curing the silicone fluid in 29.5-mm-diameter, 1.5-mm-deep cylindrical poly(tetrafluoroethylene) (PTFE) molds. The samples were cured at room temperature for 15 h. This resulted in the production of 1-mm-thick elastomer samples that were smooth and uniform in thickness. The cylindrical samples were then cut into 10-mm-wide stripes and clamped into a custom-built stretching rig. This stretching rig consisted of an adjustable sample holder that was used to stretch the elastomer test pieces to a desired prestrain ε_{pre}. The adjustable sample holder was mounted onto a separate detachable base that contained a micrometer for precision stretching of the elastomer samples (Figure 1a). In these experiments, the initial length of the elastomer test piece, $L_o(x)$, was fixed to ensure that a uniform strain was applied to the samples. Once stretched by an amount ΔL, the adjustable sample holder could be locked in place using set screws and then removed from the baseplate without the dimensions of the elastomer samples changing. The detachable sample holder was designed so that it was small enough to fit into the sample holder in the bell jar of a thermal evaporation unit. The design of the sample holder also ensured that it could be placed under the objective of an optical microscope.

Prestrain values in the range of $1\% < \varepsilon_{pre} < 60\%$ were applied to the elastomer samples. Following the application of the prestrain, thin capping layers of high-purity aluminum (Al, Advent Ltd., U.K., 99.999%) with thickness values in the range of 20−500 nm were thermally evaporated on top of the elastomer films. Evaporation was performed under vacuum ($< 10^{-5}$ Torr) at a temperature of 50 °C. The thickness of the Al capping layer was measured in situ by monitoring changes in the resonance frequency of a quartz crystal that was mounted close to the elastomer sample in the evaporation chamber. The thickness of the Al layers was also calibrated by evaporating films onto single-crystal silicon wafers (Compart Technology, U.K.) and measuring the thickness of a masked region of the film using an Asylum Research MFP-3D scanning force microscope operating in intermittent contact mode.

When the Al-capped elastomer samples were removed from the evaporator, the prestrain in the silicone elastomer was released. Prior to release, the Al capping layer was in a state of zero stress. However, when the elastomer relaxed, the Al capping layer was left in a state of compressive stress. The compression of the thin Al capping layers by the relaxing elastomer layers resulted in the formation of sinusoidal surface wrinkles with wavelengths in the 3−42 μm range and amplitudes in the 0−3.6 μm range (Figure 1). These wrinkles were oriented perpendicular to the direction of the applied prestrain. Some cracking of the capping layers was observed at prestrain values of 10% and above (Figure 1b). This crack formation occurred parallel to the direction of the applied prestrain and was attributed to yield processes in the Al capping layers. The crack density was observed to increase with the magnitude of the applied prestrain.

Samples with gradients in the wrinkling length scale were produced by adjusting the angle of the clamps on the sample holder such that the free region of the unstretched elastomer between the two clamps was trapezoidal in shape. This meant that the initial (unstretched) length of the samples, L_o, depended upon the position, x, on the sample (Figure 1a). When the elastomer samples were stretched by a fixed amount ΔL, the variation in the unstretched length caused the prestrain in the samples to vary according to position such that $\varepsilon_{pre} = \Delta L/L_0(x)$. Prior to the release of the prestrain, thin Al capping layers of uniform thickness were deposited on top of the elastomers using identical deposition parameters to those described above. Because both the amplitude and the wavelength of the pattern are dependent upon ε_{pre} (eqs 1 and 2), the local variations in the applied prestrain resulted in a gradient in these measured length scales across the surfaces of the samples.

All of the Al-capped elastomer samples were imaged using an Olympus BX51 optical microscope using bright-field illumination and differential interference contrast (DIC) (Figure 1b). The wavelength of the wrinkles on a given sample was obtained by Fourier transformation of the resulting micrographs. The wavelength, λ, and its associated uncertainty, $\Delta\lambda$, were obtained from the position, k_{max}, and width, Δk, of the dominant peak in the radially averaged Fourier transform (Figure 1d,e) using the expressions $\lambda = 1/k_{max}$ and $\Delta\lambda = \Delta k/k_{max}^2$, respectively. This process was repeated at different locations on the surface of each sample to test the reproducibility of the measured length scales. Measurements of the wrinkle amplitude and wavelength were also obtained from scanning force microscopy scans of each sample (Figure 1c). In each case, line profiles were obtained from the scans and were used to confirm the wrinkle wavelength values obtained using optical microscopy and to measure the amplitude of the sinusoidal corrugations/wrinkles (Figure 1c). The data points in Figures 2 and 3 show the thickness and prestrain dependence of the wrinkle wavelengths and amplitudes that were obtained on samples with uniform strains. The solid lines in these Figures represent theoretical predictions that were calculated using the model developed by Song et al.[27] (eqs 1 and 2). Figure 4 shows measurements and calculations of wrinkle wavelength and amplitude values as a function of position for a sample with an applied strain gradient where the prestrain varies from ~100 to ~10% over a distance of 16 mm.

The values of E_{cap}, ν_{cap}, and ν_{sub} used to calculate the solid lines in Figures 2−4 were obtained from the literature.[33−35] The value that was used for the Young's modulus of the evaporated Al capping layers, E_{cap}, was 30 GPa rather than the bulk value for aluminum (70 GPa). This was done because Read et al.[34] and Hoffman[35] have shown that in evaporated thin films the Young's modulus of Al is reduced by the presence of small Al grain sizes within the films. The value of the Young's modulus of the elastomer, E_{sub}, was obtained from axisymmetric deformation tests that were based upon the method developed by Johnson, Kendall, and Roberts.[36−38] The samples for these experiments were prepared by curing the silicone elastomer in 11.2-mm-diameter hemispherical PTFE molds at room temperature for 15 h. The samples were then released and placed on top of a digital balance that was in turn placed on top of a laboratory jack (inset in Figure 5). The sample was then raised until it made contact with the bottom surface of a clean glass microscope slide that was coated with a thin, uniform layer of silicone (prepared by spin coating). At this point, a circular contact patch developed between the hemispherical elastomer sample and the silicone-coated glass slide, and a force was measured by the digital balance. The radius of the contact patch, a, was varied by adjusting the height of the laboratory jack and measured using a traveling microscope. At each point, a measurement of the applied load, F, was obtained using the digital balance.

(33) *Polymer Handbook*; Brandrup, J., Immergut, E. H., Grulke, E. A., Eds.; Wiley: New York, 1999.
(34) Read, D. T.; Cheng, Y.-W.; Keller, R. R.; McColskey, J. D. *Scr. Mater.* **2001**, *45*, 583–589.
(35) Hoffman, R. W. *Mater. Res. Soc. Symp. Proc.* **1989**, *130*, 295–306.
(36) Johnson, K. L. *Contact Mechanics*; Cambridge University Press: Cambridge, England, 1985.
(37) Maugis, D. *Contact Adhesion and Rupture of Elastic Solids*; Springer: Berlin, 1934.
(38) Shull, K. R.; Chen, W. *Interface Sci.* **2000**, *8*, 95–100.

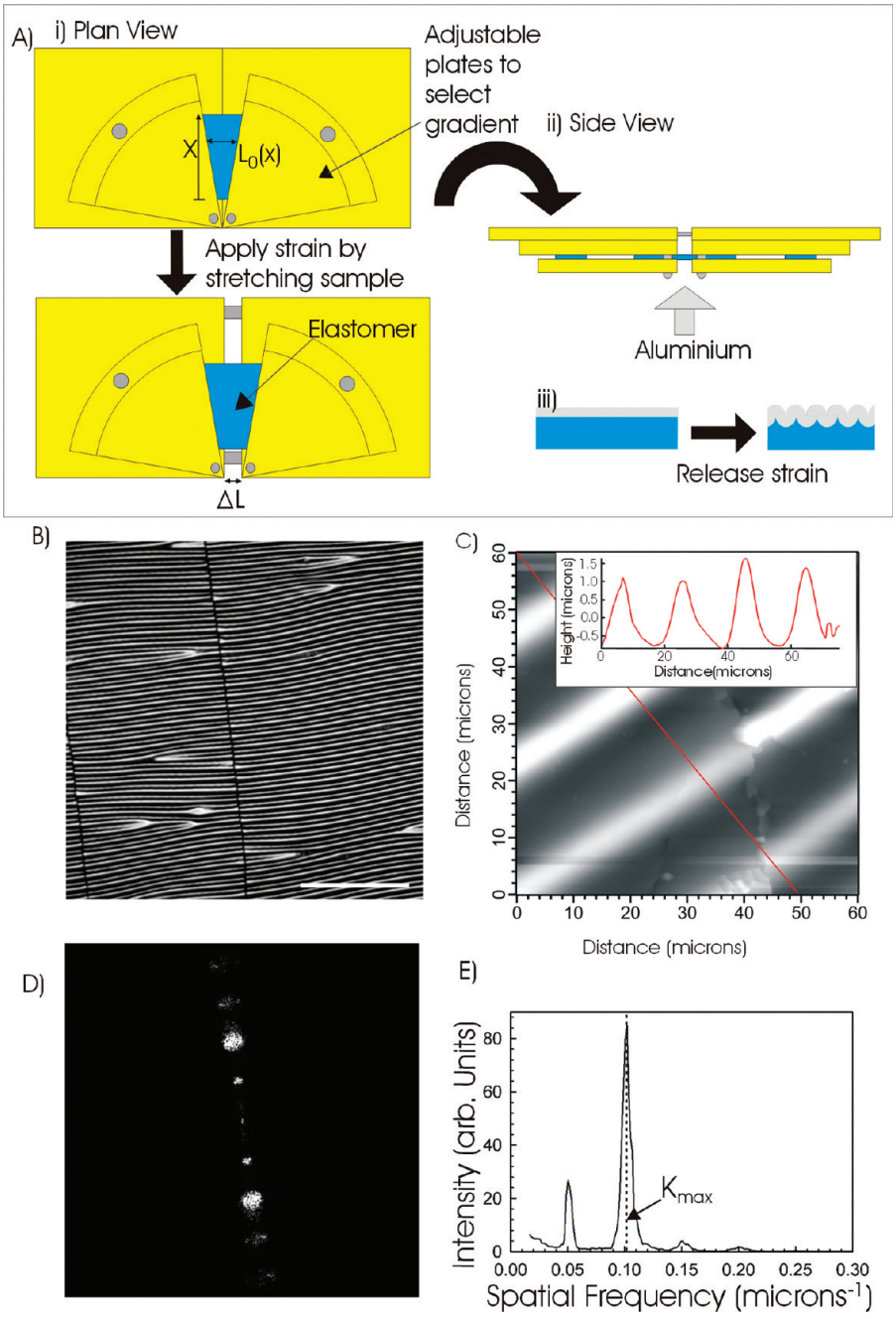

Figure 1. (A) Schematic diagram of the stretching rig used to apply a prestrain to the elastomer during the evaporation of Al. (i) Plan view of the stretching rig. An elastomer sample is clamped in place before being stretched by ΔL to apply a prestrain of $\varepsilon_{pre}=\Delta L/L_0(x)$. (ii) Side view of the stretching rig. Al is evaporated onto the elastomer sample. (iii) The strain is then released, causing the bilayer to wrinkle. (B) Microscope image of a patterned elastomer−Al bilayer (10% prestrain, 150-nm-thick Al layer, scale bar 200 μm). (C) Scanning force microscopy image of the same bilayer shown in image B. Also shown is the location of the inset scanning force microscopy line profile. (D) Fast Fourier transform of the microscope image shown in image B. (E) Radial average of the Fourier transform shown in part D. The position of the dominant peak, k_{max}, is used to calculate the wavelength of the wrinkles on a given sample. (See the text.)

The applied load is related to the contact radius by the equation[38]

$$F = \frac{16Ea^3}{9R} - \left(\frac{32\pi EGa^3}{3}\right)^{1/2} \quad (3)$$

where R is the radius of curvature of the hemisphere and G is the work of adhesion (J m^{-2}) between the hemisphere and silicone-coated glass surfaces. Figure 5 shows a plot of the applied load as a function of a^3 along with a fit to the form of eq 3. The Young's modulus of the elastomer obtained from these measurements was $E = E_{sub} = 2.11 \pm 0.08$ MPa. This was found to be in agreement with the range of values quoted for silicone elastomers.[33] A value for the work of adhesion between the silicone hemisphere and the silicone-coated glass surface was also obtained and was found to be $G = 1.1 \pm 0.8$ J m^{-2}. However, we note that G is not needed for the analysis of the wrinkle data and will not be discussed any further.

The wetting properties of the wrinkled and gradient samples were also studied by measuring the contact angles of small sessile water droplets that were placed on their surfaces. This was done by placing the samples on a level surface and then observing the droplets from the side using a Philips SPC 1030NC webcam.

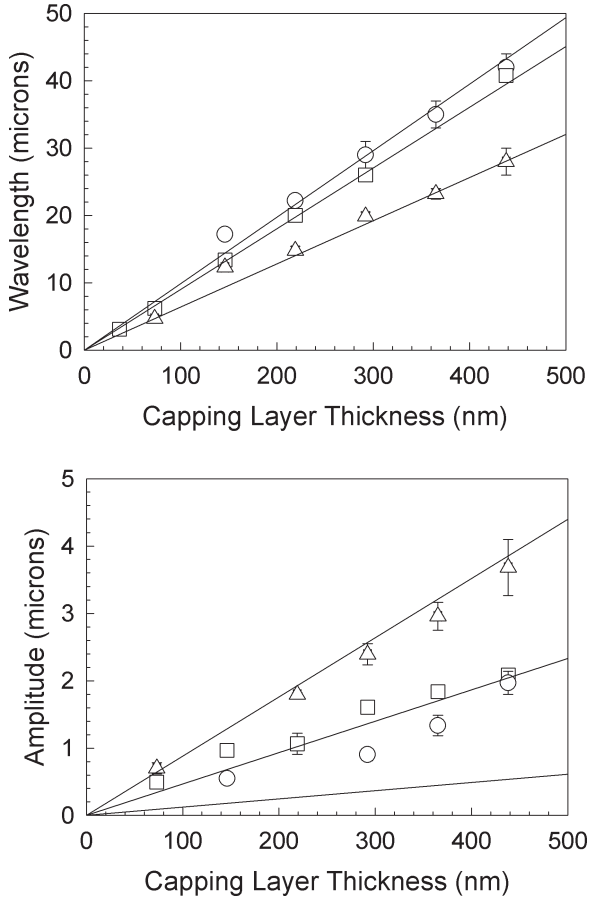

Figure 2. Al capping layer thickness dependence of the wrinkle wavelength (top) and amplitude (bottom) measured for prestrains of 1 (○), 10 (□), and 50% (Δ) respectively. Also shown are the predictions of the Song et al.[27] model (−).

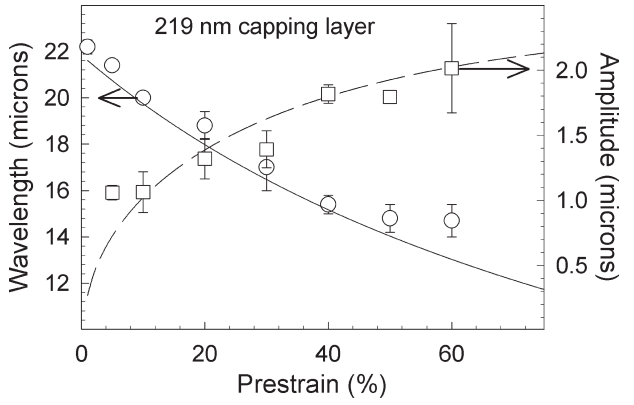

Figure 3. Prestrain dependence of the wavelengths (○) and amplitudes (□) of wrinkles on elastomer samples that were capped with a 219-nm-thick layer of Al. Also shown are the predictions of the Song et al.[27] model for the wavelength (−) and amplitude (---).

Images of the droplets were obtained, and the contact angles were measured using software written in Matlab (MathWorks). The uncertainties associated with the contact angles obtained using this method were found to be ±1°. The motion of harmonically vibrated water droplets on gradient samples that had been mounted on the surface of a loudspeaker was also observed using an optical microscope.

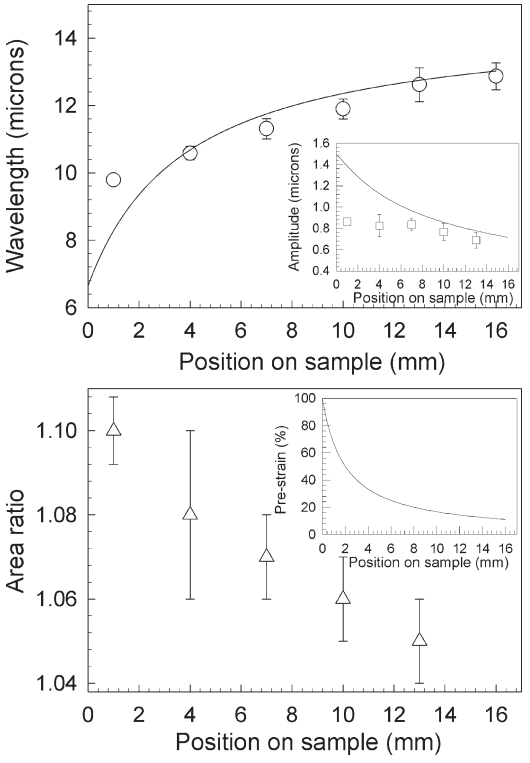

Figure 4. Topographic properties of a gradient sample. The top panel shows the wavelength and amplitude (inset) at selected positions on the surface of the sample. The predictions of the Song et al.[27] model are also shown at each position (−). The bottom panel shows the surface area ratio as a function of position. (See the text.) The inset in the bottom panel shows how the strain in the sample varies with position.

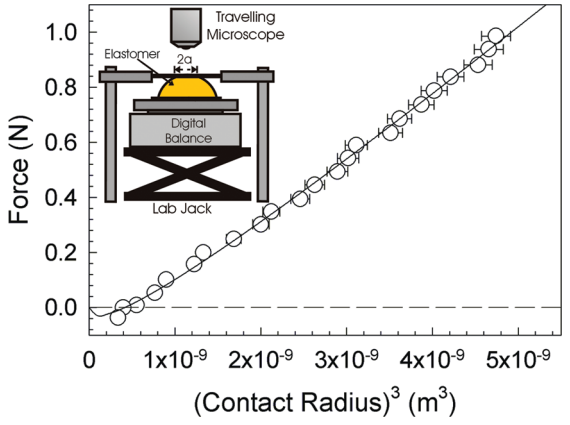

Figure 5. Axisymmetric deformation data used to determine the Young's modulus of the cured silicone elastomer. A fit of this data to eq 3 gives $E = 2.11 \pm 0.08$ MPa. A schematic diagram of the experimental setup used to measure these data is shown as an inset.

Results and Discussion

Figures 2 and 3 show good quantitative agreement between experiment and calculations of the wrinkle wavelengths and amplitudes when the measured value of E_{sub} of the silicone elastomer and the value of E_{cap} given by Read et al.[34] are used in eqs 1 and 2. The only exception to this is the difference between the amplitude data for samples with 1% prestrain and the predictions of the model by Song et al.[27] that are shown in Figure 2. The differences that are observed at this low prestrain are likely to be due to uncertainties in the strain that arise from

heating the elastomer samples during the evaporation of Al. However, small variations/uncertainties in the applied prestrain may also have a measurable effect in this regime. Thermal expansion is expected to increase the effective prestrain in the elastomer. When the Al capping layer is deposited, the samples are cooled, and the strain is released, there will be an additional component of the applied stress that occurs because of the mismatch in expansion coefficients of Al and the elastomer. This difference in thermal expansion coefficients, $\Delta\alpha$, is expected to introduce an additional thermal strain within the Al on the order of $\varepsilon_T = \Delta\alpha\Delta T$, where ΔT is the change in temperature of the elastomer during thermal evaporation of the Al layers. Typical values for the expansion coefficients of Al and silicone elastomers were found to be 2.3×10^{-5} and 3.1×10^{-4} K^{-1},[39] respectively, and the rise in temperature in the sample was measured in situ to be 25 K. This gives a value for the thermal strain of 0.7%, which is comparable to the 1% prestrain that was applied to the samples. Calculations based upon eqs 1 and 2 show that the increase in strain caused by the temperature difference is expected to increase the amplitude of the surface corrugations/wrinkles on the samples with a 1% prestrain by a factor of ~1.3 and to decrease the wavelengths by a factor of 0.99. At prestrains of 10% and higher, similar calculations show that the effects of thermally induced strains on both the measured amplitudes and wavelengths are expected to be negligible. The observed differences between the 1% prestrain amplitude data are clearly larger than the predictions of the model by a factor of ~2 to 3. Similar deviations at low prestrains are also observed in Figure 3, which shows the strain dependence of the wrinkling wavelength and amplitude for samples with 219-nm-thick capping layers. Calculations based upon the results obtained for the amplitudes of the samples with 1% prestrain shown in Figure 2 suggest that the uncertainty in the effective applied strain due to changes in temperature and other strain mechanisms is as high as ±3%.

Figure 4 shows data for the amplitude and wavelengths of the wrinkles on a sample where the applied strain was varied between 100 and 10% over the length of a 16 mm elastomer sample. The variation of prestrain with position on the sample is shown as an inset in the bottom panel of this Figure. The top panel shows the measured wavelength and amplitude data (inset) as a function of position on the sample. As expected, on the basis of the results shown in Figures 2 and 3, the wavelength of the wrinkles decreases and the amplitude increases in regions of the sample that were subjected to higher prestrains. The solid lines in this Figure show that quantitative agreement was also observed between the predictions of eq 1 and the measured wavelengths on the gradient samples (Figure 4). The measured amplitude values are lower than those predicted by eq 2; however, they still vary by a quantifiable amount that is larger than the experimental uncertainties. We stress at this point, however, that the model developed by Song et al.[27] describes the evolution of surface wrinkles in samples that have been exposed to a uniform prestrain. It is not clear at this stage how this model should be modified (if at all) to incorporate the effects of strain gradients in the samples. However, the level of agreement that has been obtained between the measured and calculated wavelength data for the gradient samples suggests that this model provides a good approximation to the measured length scales in strain gradient samples.

The bottom panel in Figure 4 shows how the surface area of the gradient samples varies as a function of position. The data points shown in this panel were calculated using the experimental amplitude and wavelength data. These values were used to determine a quantity called the area ratio, r, which is defined as the surface area of the wrinkles per unit area on the substrate and is calculated using the equation

$$r = \frac{L\int_0^L \left(1+\frac{dz^2}{dx}\right)^{1/2} dx}{L^2} = \frac{\int_0^L \left(1+\frac{dz^2}{dx}\right)^{1/2} dx}{L} \quad (4)$$

where L^2 is the area of a region on the substrate, $z(x) = A \sin(2\pi x/\lambda)$, and x is the position on the substrate measured in a direction perpendicular to the direction of the wrinkle/groove axis. The values of the area ratio shown in Figure 4 demonstrate that the area of the wrinkled surface varies linearly with position on the strain gradient sample. These local variations in surface area are expected to influence the wetting properties of small droplets that are placed on the surfaces of the samples because the area of contact between the base of a sessile liquid droplet and the substrate will be dependent on position. Local differences in the contact area between a drop and the surface are expected to influence the energy associated with the liquid/substrate interface. If the surface area that a droplet "feels" changes over length scales that are comparable to the dimensions of the drop, then the balance of interfacial energies will be different at opposite ends of the droplet along the direction of the gradient in length scales. Such an imbalance in the interfacial energies will lead to a measurable difference in the contact angles on either side of the droplet. Figure 6 shows images of sessile water drops that have been placed on samples that have been subjected to uniform applied prestrains (Figure 6a,b) as well as an image of a water drop on a strain gradient sample (Figure 6c). The droplets on the uniform prestrain samples had measured contact angles of 96.1 ± 0.5 and 134.6 ± 0.5°, respectively, and these were found to be the same on both sides of the droplets within the limits of experimental uncertainty. The droplet on the gradient sample was observed to have two distinct contact angle values, thus indicating that these samples do have gradient wetting properties. On the side of the droplet where the area of the liquid/substrate interface was higher (high substrate prestrain), the measured contact angle was 112 ± 1°. On the other side of the droplet, corresponding to the low substrate prestrain, the measured contact angle was 109 ± 1°.

As discussed above, the presence of a wetting gradient is expected to result in an imbalance in the interfacial energies on either side of the droplet. Such an imbalance in interfacial tension would result in a net force being exerted on the liquid droplets. This is expected to be the case for the gradient samples discussed above. However, the forces that are exerted on the drop are often not sufficient to overcome the effects of contact line pinning when the edge of the droplet reaches a defect on the substrate surface.[29] These pinning effects can often be overcome by vibrating the droplets close to their resonance frequency. Vibrations can be applied in a direction either perpendicular[40] or parallel[32,40−42] to the surface of the sample. Under these circumstances, the small bias in the wetting properties of the substrate causes the droplets to move down the wetting gradient from regions of high to low interfacial energy.[29,32] Figure 7 shows microscope images of a droplet on one of the gradient samples described above. The sample in these images was placed on the surface of a horizontally

(39) Govindaraju, A.; Chakraborty, A.; Luo, C. *J. Micromech. Microeng.* **2005**, *15*, 1303–1309.

(40) Noblin, X.; Kofman, R.; Celestini, F. *Phys. Rev. Lett.* **2009**, *102*, 194504.

(41) Daniel, S.; Chaudhury, M. K.; deGennes, P. G. *Langmuir* **2005**, *21*, 4240–4248.

(42) Dong, L.; Chaudhury, A.; Chaudhury, M. K. *Eur. Phys. J. E* **2006**, *21*, 231–242.

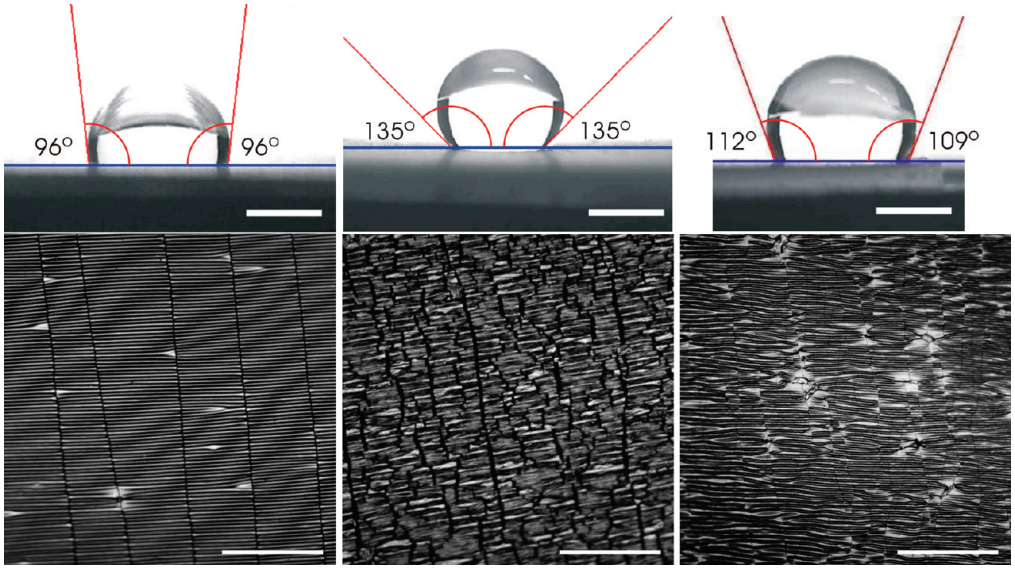

Figure 6. Examples of sessile water droplets on uniform and gradient surfaces as viewed from the side (top panel). A scale bar of 1 mm is shown at the bottom left of each image. The bottom panels show micrographs of the sections of the sample on which the droplets were placed taken prior to deposition of the droplet (scale bar 200 μm). The prestrain and capping layer thickness of each sample is as follows: (left) 10% prestrain, 146 nm capping layer, and a contact angle of $96 \pm 1°$; (middle) 90% prestrain, 146 nm capping layer, and a contact angle of $135 \pm 1°$; and (right) gradient sample with a 146 nm capping layer with strain going from 10% at the low-strain end to 100% at the high-strain end (90% prestrain at the displayed position). The right-hand contact angle is $109 \pm 1°$, and the left-hand contact angle is $112 \pm 1°$.

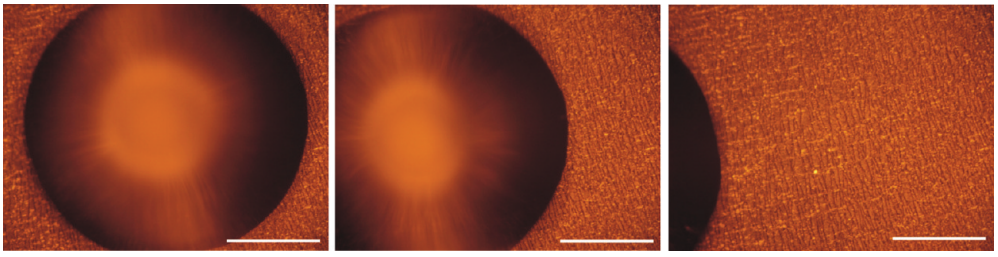

Figure 7. Images showing the movement of a 10 μL sessile water droplet on a gradient surface where the droplet was vibrated close to its resonance frequency (210 Hz). The images are taken in order from left to right with a 2 s interval. The average speed of the droplet was over 200 μm/s. Scale bar 500 μm.

mounted loudspeaker and then leveled. A 10 μL water droplet was then placed at the high-strain (high-surface-area) end of the substrate, and the substrate was vibrated at a frequency of ~210 Hz (corresponding to the resonance frequency of the droplet[43,44]). The images in Figure 7 show that as the droplet is vibrated it moves rapidly down the wetting gradient and that the droplets move with speeds in excess of 200 μm/s. This elegant demonstration confirms the feasibility of using the strain gradient samples as surfaces for directing the motion of small liquid droplets. In contrast, no motion was observed for droplets that were placed on wrinkled surfaces where no gradient was present (i.e., when the wrinkle wavelengths and amplitudes were the same everywhere on the sample; see Supporting Information).

It is not clear what role the cracks that form in the capping layers play in influencing the motion of liquid droplets. As shown in Figure 6, the crack density in the Al capping layers increases with increasing prestrain. This increase in crack density is also expected to increase the effective surface area of samples at higher prestrain values. Higher crack densities might therefore be expected to result in larger contact angles and a gradient in the crack density would result in a gradient in the wetting properties. In this respect, the effects of cracking in the Al films would be almost indistinguishable from those due to wrinkling, except that the jagged crack surfaces may be expected to pin the three-phase contact lines of droplets more efficiently. The focus of future work will be to determine the effects of replacing the Al capping layers with glassy polymer layers such as polystyrene or poly(methylmethacrylate), which are more likely to yield and flow than to crack. We hope that these future experiments will enable us to decouple effects due to crack-induced effects and those that are related purely to gradients in the wrinkling length scales. However, regardless of the dominant mechanism for creating wetting gradients on these samples, the final result is the same! Al/silicone elastomer bilayer samples that have been subjected to a strain gradient during manufacturing result in the production of topographically structured surfaces that have a gradient in the local surface area. This gradient influences the wetting properties of small liquid droplets and can be used to direct their motion when a small external perturbation such as an out-of-plane vibration of the sample is applied.

Conclusions

Prestrained elastomer samples were capped with thin Al films, and the strain was released to produce uniform sinusoidal surface wrinkles whose amplitude and wavelength were found to depend

(43) Noblin, X.; Buguin, A.; Brochard-Wyart, F. *Eur. Phys. J.* **2009**, *166*, 7–10.
(44) Chandrasekhar, S. *Proc. London Math. Soc.* **1959**, *3*, 141–149.

upon the thickness of the Al capping layer and the magnitude of the applied prestrain. The results obtained for the measured wavelengths and amplitudes were found to be in good agreement with the predictions of a recent model of wrinkle formation in strained elastomers that are capped with rigid overlayers. Samples with gradients in the wrinkling length scale were also manufactured by applying a strain gradient to the elastomer prior to deposition of the Al capping layers. The amplitudes and wavelengths measured on these gradient samples were also found to be consistent with theoretical predictions. The gradient samples were shown to result in an imbalance in the contact angles of small sessile water droplets that were placed on their surfaces. When vibrated close to the resonance frequency of the water droplet, the gradient in wetting properties of these surfaces was shown to direct the motion of the liquid drops.

Supporting Information Available: Videos showing droplet motion on a surface with uniform prestrain (video is at 10 times real speed) and droplet motion on a surface with a gradient in prestrain (video is at real speed). This material is available free of charge via the Internet at http://pubs.acs.org.